Macromolecular Rapid Communication
www.mrc-journal.de

Solvent Vapor Annealing of a Diblock Copolymer Thin Film with a Nonselective and a Selective Solvent: Importance of Pathway for the Morphological Changes

*Florian A. Jung, Anatoly V. Berezkin, Tim B. Tejsner, Dorthe Posselt, Detlef-M. Smilgies, and Christine M. Papadakis**

Diblock copolymer thin films of polystyrene-*block*-poly(dimethyl siloxane) (PS-*b*-PDMS) featuring PDMS cylinders in a PS matrix are investigated during solvent vapor annealing with mixtures of *n*-heptane (which is strongly selective for PDMS) and toluene (which is close to nonselective for both blocks). Swelling in the vapor of one of the pure solvents and exchanging it stepwise by the vapor of the other solvent is compared to swelling in a given binary solvent vapor mixture for a prolonged time. The resulting structural changes, such as ordering of the cylinders on a hexagonal lattice and their transition into lamellae, are followed using in situ, real-time grazing-incidence small-angle X-ray scattering (GISAXS). In three runs, the sequence of solvent vapor swelling and vapor exchange is varied. Compiling the resulting morphologies in a diagram of states in dependence on the solvent content in the film and in the minority nanodomains allows insight into the role of the glass transition of the PS matrix for the ordering processes and their time scales. Based on these findings, a protocol is suggested to efficiently obtain an order-to-order transition from the cylindrical morphology with random domain orientation to the oriented lamellar state.

Block copolymer thin films feature rich behavior: Not only can different nanostructures be prepared, but also the nanodomain orientation may vary and the detailed structure near the film interfaces may differ from the bulk structuring. [1–4] Nanostructured thin films have a variety of applications, e.g., as optical elements, where large structures are needed,[5] in polymer photovoltaics, where block copolymers with conductive blocks are used as a functional layer,[6] or in nanolithography, where small and perfectly ordered structures are needed.[7] Especially the cylindrical and the lamellar morphology have proven useful to create laterally structured substrates, e.g., line or dot patterns.[8–10] Typically, the thin films are prepared by spin-coating, yielding smooth films of well-defined thickness. However, the fast removal of the solvent in this technique often results in defects, hampering the applications. The importance of trapped kinetics in block copolymer processing has recently been highlighted.[11]

Solvent vapor annealing (SVA) has frequently been used for improving the degree of order or for altering the orientation of the nanodomains or even the morphology.[12–18] Typically, a solvent of high vapor pressure is chosen, and the sample is immersed for a certain time in the vapor atmosphere of the solvent, before it is dried. Various SVA setups have been designed to precisely control the processing parameters, e.g., the annealing temperature, making the method a reliable way to process block copolymer thin films for applications.[19–27] In situ experiments[28–32] and simulation studies[33–37] have been performed to elucidate the structural changes during SVA and thus to improve the understanding of the annealing process, resulting in more powerful processing protocols.

The selectivity of the solvent plays an important role for efficiently improving and/or altering the morphology of a block copolymer thin film. Using a very selective solvent may result in strong swelling of one type of nanodomains, e.g., the cylinders in a matrix formed by a compositionally asymmetric diblock copolymer, which may lead to an overall change of the type of morphology. However, if the matrix consists of a glassy polymer, such as the frequently used poly(methyl methacrylate)

F. A. Jung, Dr. A. V. Berezkin, Prof. C. M. Papadakis
Technische Universität München
Physik-Department
Physik der weichen Materie
James-Franck-Str. 1, Garching 85748, Germany
E-mail: papadakis@tum.de
T. B. Tejsner, Prof. D. Posselt
IMFUFA
Department of Science and Environment
Roskilde University
P.O. Box 260, Roskilde 4000, Denmark
Dr. D.-M. Smilgies
Cornell High Energy Synchrotron Source (CHESS)
Wilson Laboratory
Cornell University
Ithaca, NY 14853, USA
The ORCID identification number(s) for the author(s) of this article can be found under https://doi.org/10.1002/marc.202000150.

DOI: 10.1002/marc.202000150

or polystyrene (PS), and is not swollen at all by the solvent vapor, the cylinders in the example cannot swell either and stay confined. Thus, it is advisable to swell also the matrix to a certain extent, so these blocks become mobile as well, and structural rearrangements may take place on manageable time scales. The underlying reason is not only the altered space demand of the cylinders, but the also the interfacial tension and the necessity for block stretching are different as well.[38] Note that microphase separation in block copolymers is thermodynamically driven and occurs even in highly swollen films, provided the segregation is strong enough.[39] To adapt to the new conditions, individual block copolymer chains must be able to leave or join the cylindrical nanodomains and migrate through the matrix, which is not possible if the matrix is in the glassy state. However, it may be difficult to identify a solvent compatible with the process environment which has the desired qualities and selectivities for the two blocks simultaneously, combined with a sufficiently high vapor pressure.

This limitation can be overcome by using mixtures of solvent vapors of different quality and selectivity, allowing to test the role of the glass transition for the structural transformations and the resulting nature of the morphology change. For instance, one might suspect different mechanisms when the cylinders are swollen first with the matrix being glassy and then the matrix is swollen as well or when both types of nanodomains are swollen simultaneously. Such questions can be addressed by using SVA setups with two individual bubblers, each containing one of the solvents, which allows preparing vapors from different solvents independently.[14] Moreover, the composition of the vapor may be varied, and is not limited by the vapor–liquid equilibrium of a solvent mixture. It has proven attractive to combine solvents of different selectivity, especially for altering the morphology.[12,14,40] Hence, combining a solvent which is nonselective—and therefore swells both the cylinders and the matrix equally—with a solvent which is selective for the cylinders and swells these exclusively, may result not only in the healing of defects, but also in a change of morphology toward the lamellar state (the two nanodomain volumes become less asymmetric). This new morphology may be preserved by kinetic trapping via rapid removal of solvent from the film[12] or by cross-linking.[41]

To investigate the role of the solvent vapor composition and to determine the role of the solvent selectivity, it is advisable to choose a block copolymer with chemically significantly different blocks, i.e., different solubility parameters. Polystyrene-*block*-poly(dimethylsiloxane) (PS-*b*-PDMS) is a suitable candidate with a high Flory–Huggins interaction parameter ($\chi \approx 0.14$ at room temperature[7]) and Hildebrand solubility parameters, which are significantly different, namely, 18.5 $(MPa)^{1/2}$ for PS and 15.5 $(MPa)^{1/2}$ for PDMS.[14] The solvents toluene and *n*-heptane have solubility parameters of 18.3 and 15.3 $(MPa)^{1/2}$, respectively,[42] and can thus be considered as selective for either the PS or the PDMS blocks. Based on this consideration, pure toluene is expected to reduce the effective volume fraction of the PDMS nanodomains in a PS-*b*-PDMS thin film, whereas *n*-heptane is expected to significantly increase it. However, in experiments on homopolymer thin films, it was observed that toluene swells not only PS thin films, but also PDMS thin films to a certain extent, i.e., toluene is only weakly selective to PS.[14] Mixtures of vapors of toluene and *n*-heptane can thus be used to vary the overall selectivity between the ones of pure toluene and pure *n*-heptane. A wealth of morphologies was revealed in this way.[14,43,44]

Varying the vapor composition stepwise while monitoring the film morphology using in situ real-time grazing-incidence small-angle X-ray scattering (GISAXS) allows probing a large composition range efficiently. We previously carried out such experiments using SVA with toluene and *n*-heptane of a thin film from a PS-*b*-PDMS diblock copolymer (initial film thickness 187 nm, overall flow rate 100 sccm), which forms randomly oriented PDMS cylinders in a PS matrix.[26] Experiments carried out at room temperature and at 44 °C gave the same sequence of morphologies, but the higher temperature was found to accelerate the kinetics of structural rearrangement and improve long-range order. Using spectral reflectance, the film thickness was measured simultaneously with swelling, allowing determination of the polymer volume fraction in the film, ϕ_P, in situ. Interestingly, after swelling the film in *n*-heptane vapor, no transition to the lamellar morphology was observed, even though *n*-heptane is expected to swell the PDMS cylinders selectively. Exchanging the *n*-heptane vapor stepwise by toluene vapor, the lateral degree of order of the cylinders improved, and a sudden morphological transition to the lamellar structure was observed, when the mixing ratio of *n*-heptane and toluene vapor was 3:7 (which corresponds to a ratio of molar flows of ≈4.9:7). Both, lying (i.e., parallel to the film interfaces) and standing (i.e., perpendicular to the film interfaces) lamellae were present in the film. Thus, the presence of toluene enabled swelling of the PS matrix and made it sufficiently mobile to enable the PDMS cylinders to transform into lying and standing lamellae. Upon further exchange of *n*-heptane by toluene vapor, the lamellae transformed into hexagonally packed standing and lying cylinders, and finally, only lying cylinders "survived," before the disordered state was encountered. During rapid drying, lying cylinders reappeared. This novel type of experiments allowed probing a trajectory in the state diagram of the PS-*b*-PDMS/*n*-heptane/toluene mixture, which was drawn in dependence on ϕ_P and the effective volume fraction of the swollen PDMS nanodomains (i.e., including solvent), f_{eff} (such a representation is named "diagram of states" hereafter). The solvent distribution in the two types of nanodomains was estimated from the intensities of the Bragg reflections in the 2D GISAXS maps along with the overall swelling ratio of the film.

In the present work, we report on three more SVA sequences. In each sequence, we target the 3:7 ratio of vapor flows, which previously resulted in the morphological transition to lamellae. A comprehensive diagram of states is constructed from the results, including order-to-order transitions and the regions where PS is glassy. Moreover, the role of the specific pathway is discussed. Thin films are prepared from the same PS-*b*-PDMS diblock copolymer in the same way as reported previously.[26] We approach the targeted ratio in three different ways, namely by swelling in a 3:7 vapor mixture of *n*-heptane and toluene for prolonged time; by swelling in toluene for prolonged time and exchanging it by *n*-heptane until the 3:7 ratio is reached; and by following the same protocol once more, but continuing the

exchange until the vapor consists of *n*-heptane exclusively and then installing the 3:7 ratio once more.

The paper is structured as follows: the swelling behavior and morphological changes in the three experiments are discussed along with the solvent distribution. For each experiment, the trajectory in the diagram of states is drawn together with the morphologies. Finally, the three experiments are compared with the one reported previously to draw general conclusions about the morphological changes in dependence on the pathway of swelling and solvent exchange. The results lead us to suggest an efficient protocol for achieving a morphological transition as well as orientational order. A brief description of the sample preparation and the SVA experiments is given in the Experimental Section.

To elucidate the role of the specific SVA pathway of thin films of a cylinder-forming diblock copolymer with a vapor from two solvents having different selectivities toward the two blocks, the following three experiments on identically prepared thin films were carried out

i. A film was swollen in a vapor having an *n*-heptane/toluene ratio of 3:7 and was kept there for ≈3000 s. Then, the film was dried slowly by reducing the flow rates of both vapors equally over more than 1500 s and, at the same time, increasing the N_2 flow while keeping the overall gas flow constant. Of the three experiments, this experiment gives the swollen film maximum time at the mixing ratio of 3:7 as well as maximum time for drying.
ii. A film was swollen in toluene for ≈3000 s. Then, toluene was exchanged by *n*-heptane, until an *n*-heptane/toluene ratio of 3:7 was reached. Again, the total gas flow was kept constant. After 300 s at this mixing ratio, the film was dried rapidly. In this experiment, the initial swollen state is different from our previous experiment (i), and we expect that the PDMS cylinders and the PS matrix swell almost equally in the toluene vapor. Exchange by *n*-heptane is expected to swell the PDMS cylinders additionally before installing the mixing ratio of 3:7.
iii. A film was swollen in toluene for ≈3000 s as in (ii); then, toluene was exchanged completely by *n*-heptane over a period of ≈2700 s. The film was kept in pure *n*-heptane vapor for ≈1000 s. Afterward, a vapor with an *n*-heptane/toluene ratio of 3:7 was installed for ≈1200 s. Then, the film was dried rapidly. In this experiment, the same initial conditions as in experiment (ii) were installed, but equilibration in pure *n*-heptane was added, and the sample was kept longer at the mixing ratio *n*-heptane/toluene of 3:7.

The films have thicknesses of 179–200 nm, which corresponds to 5–6 times the cylinder repeat distance of 30 nm.[26] For each protocol, we discuss the behavior of the film thickness and identify the morphologies and orientations from the 2D GISAXS maps and the corresponding lateral 1D intensity profiles. The distribution of the two solvents in the PDMS nanodomains and the PS matrix as well as the trajectories in the diagram of states are determined. Finally, we compare the trajectories of these three and the previous experiment (introduced in the Supporting Information of ref. [26]) and identify aspects of equilibrium and kinetics.

Protocol (i): Swelling was carried out in a flow of 15 sccm *n*-heptane and 35 sccm toluene, i.e., a ratio of 3:7, for 3000 s (**Figure 1**a). The swelling ratio S_R increases, first rapidly and after ≈1500 s approximately linearly, until a value of 1.6 is reached at the end of the swelling step. The intensity profiles as well as the lateral repeat distance and grain size, which result from fitting of the intensity profiles along q_y using Equation (1) (see below), are shown in Figure S2 (Supporting Information), and the fitting parameters are compiled in Table S1 in the Supporting Information. Good agreement is obtained. During the first 600 s of swelling, the lateral repeat distance increases to ≈33.4 nm and then stays constant. Closer inspection shows that the increase of the lateral repeat distance is delayed by ≈100 s compared to the swelling of the film (inset in Figure S2b in the Supporting Information). This is related to the glass transition of PS and will be discussed in more detail below. The grain size increases after ≈300 s of swelling to ≈160 nm and then steadily to ≈220 nm, i.e., the lateral correlation of the cylinders improves. During this swelling step, the 2D patterns do not change significantly (**Figure 2**, 153–3131 s): Only a flattening of the ring in q_z direction with time is observed, indicating an increase of the cylinder spacing normal to the substrate. The intensity of the reflection does not change significantly either (Figure S2c in the Supporting Information), indicating that the scattering contrast is nearly unchanged.

The resulting reduced volumes (Figure 1b), calculated as detailed below and in ref. [26], show that *n*-heptane does not enter the PS matrix at all, but only the PDMS cylinders, as expected (the reduced volume reaches a maximum value of 0.37). The transient maximum of $\nu_{hep(PDMS)}$ at ≈280 s is presumably due to *n*-heptane being adsorbed on the inner tube walls from a previous run and now being released by the gas flow. In contrast, toluene swells PS and PDMS equally, its reduced volumes (for the definition see Equation (4) below) at the end of the swelling step are 0.55 in PS and 0.47 in PDMS. The value of $\nu_{tol(PS)} = 0.16$ at which the PS matrix is expected to cross the glass transition, i.e., to be in the viscoelastic regime, is reached after ≈350 s. This value corresponds to the onset of the changes in the lateral repeat distance described earlier. In the corresponding diagram of states (Figure 1c), the swelling of PS-*b*-PDMS according to protocol (i) leads to a downward trajectory along the ϕ_P axis until a value $\phi_P = 0.62$ is reached with the effective volume fraction of the PDMS nanodomains, f_{eff}, varying only between ≈0.36 and 0.40. We note that, even though f_{eff} increases slightly during swelling, the film maintains the cylindrical morphology, and no transition to the lamellar morphology is observed. Thus, the fraction of *n*-heptane is too small to raise f_{eff} in a way that a morphology change is induced. Moreover, the time-resolved results for the lateral repeat distance and the grain size as well as for the reduced volumes show that equilibrium is reached only after 600 s (lateral repeat distance) or even a longer time (more than 3000 s for the grain size and for $\nu_{hep(PDMS)}$).

Drying was carried out in 10 steps of 150 s, decreasing both vapor flows evenly to zero and increasing the flow of dry N_2 gas from zero to 50 sccm, keeping the overall flow constant. The swelling ratio decreases, first rapidly, then more slowly and reaches a value of 1.03. The ring in the 2D GISAXS map does not change shape, and the intensity stays roughly the same. The lateral repeat distance increases within 600 s to ≈34.7 nm, where it stays constant. The apparent change of repeat distance may be due to a change of cylinder orientation toward lying

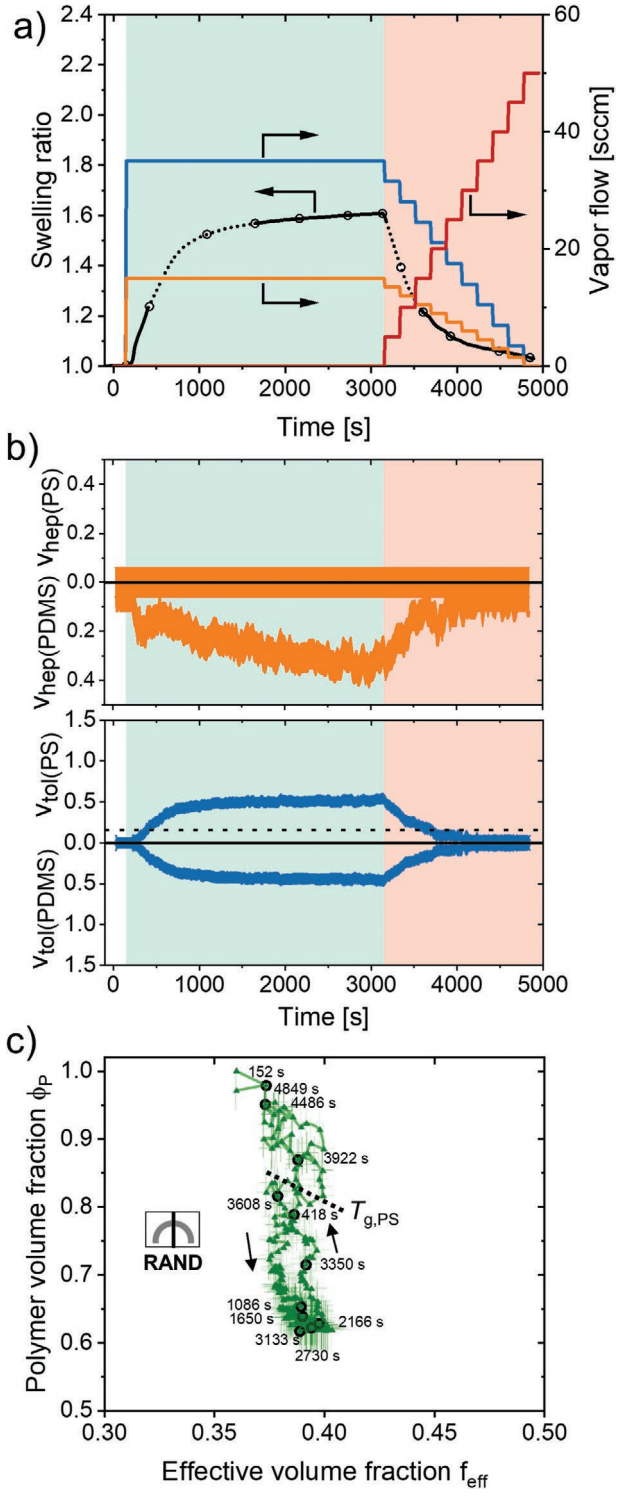

Figure 1. Protocol (i). a) Variation of the vapor flows (brown: *n*-heptane, blue: toluene, red: pure N_2 gas, all right axis) and the resulting overall swelling ratio S_R (full black line, left axis) with time. The dotted black line is based on an estimated film thickness due to a temporary failure of the spectroscopic reflectometer. Open circles indicate the times of selected 2D GISAXS maps shown in Figure 2 and Figure S2 in the Supporting Information. b) Reduced volumes of *n*-heptane and toluene in the PDMS nanodomains and the PS matrix, as estimated from the intensity of the Bragg reflection and the swelling ratio of the film. Note that the ordinates in (b) point both upward and downward. The value of $v_{tol(PS)}$ at which PS crosses the glass transition is indicated by a dotted line. c) The trajectory of the system during SVA, as described in the text, as a function of the effective volume fraction of the PDMS nanodomains, f_{eff}, and the volume fraction of polymer in the swollen film, ϕ_P. The times after the beginning of the experiment are given in the graph. The times at which the glass transition of PS is crossed upon swelling and drying are indicated by a dotted line. The film consists of randomly oriented cylinders (RAND) during the entire time, as indicated by the schematic 2D GISAXS map. Error bars are shown for every second data point. Open circles indicate the times of the 2D GISAXS maps and intensity profiles shown in Figure 2 and Figure S2 (Supporting Information).

cylinders during drying. The grain size decreases during the same time to ≈160 nm, which is slightly higher than the value before SVA (≈110 nm), i.e., the lateral correlation has improved. The reduced volumes of the solvents go smoothly to zero. In the state diagram, the trajectory moves upward along the ϕ_P axis with f_{eff} being constant. Finally, ϕ_P amounts to 0.96 and f_{eff} to 0.37.

The results of protocol (i) show that swelling a cylinder-forming PS-*b*-PDMS thin film in a 3:7 mixture *n*-heptane/toluene results in a stress relief due to the plasticization of the PS matrix. Thus, the lateral grain size increases. At the end of the swelling step, the film has taken up ≈40 vol% of solvents, and *n*-heptane has selectively swollen the PDMS cylinders, whereas toluene has swollen both PS and PDMS nearly equally. The amount of *n*-heptane is not sufficient to induce structural changes, resulting in an almost vertical trajectory in the diagram of states. Slow drying does not alter the morphology significantly, except for a slight transition toward the lying cylinder orientation and a smaller grain size than in the swollen state. A similar experiment was carried out previously on a PS-*b*-PDMS film with similar composition and film thickness, but lower diblock copolymer molar mass (16 kg mol^{-1} vs 39.5 kg mol^{-1} in the present work), and a 1:5 *n*-heptane/toluene liquid mixture for SVA.[43] The results obtained are consistent with ours.

Protocol (ii): To approach an *n*-heptane/toluene ratio of 3:7—where the transition to lamellae appeared previously—in a way different from our previous work[26] and from protocol (i), we chose to swell a film first in pure toluene for 3000 s and only afterward replace toluene by *n*-heptane until the ratio 3:7 is reached (**Figure** 3a). The latter exchange was carried out in 3 steps of 300 s. We expect that, in the toluene vapor, the PDMS cylinders and the PS matrix swell nearly equally, i.e., the PS matrix crosses the glass transition and is sufficiently mobile to allow swelling of the cylinders toward the lamellar state when exchanging toluene partially by *n*-heptane. Afterward, the film was dried rapidly.

During the initial swelling step in toluene, where a flow rate of 50 sccm was applied for 3000 s, S_R increases to a value of 2.2. Again, Equation (1) is fitted successfully to the intensity profiles along q_y, in some cases with an additional Gaussian (Equation (S4), Figure S3a, and Table S2 in the Supporting Information). During the first 650 s of swelling, the lateral repeat distance increases rapidly to 32.9 nm and then, more slowly, to 35.5 nm during the remaining time (Figure S3b,c in the Supporting

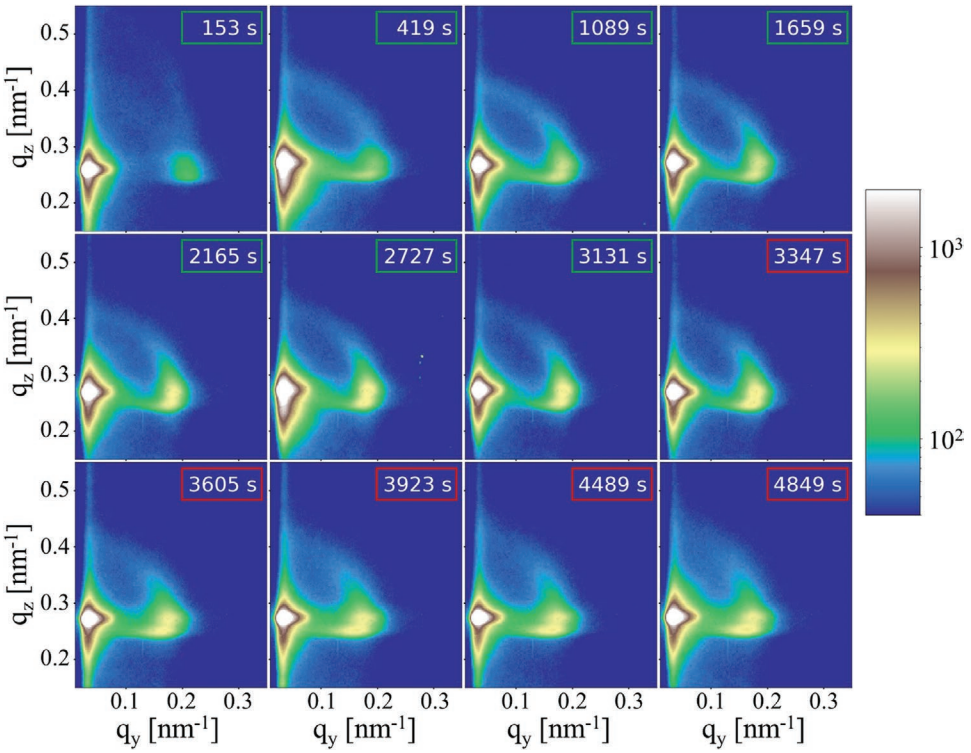

Figure 2. Protocol (i). Selected measured 2D GISAXS maps at the times given. Positive q_y values are shown. Colored frames around the times indicate the two stages of the protocol: green: swelling in *n*-heptane/toluene 3:7, red: drying. The scale bar gives the logarithmic intensity color map. For an assignment of the features see Figure S1 in the Supporting Information.

Information). The grain size increases rapidly from ≈110 to ≈150 nm and then stays constant (Figure S3b in the Supporting Information). Again, a small delay (≈100 s) in the increase of the lateral repeat distance due to the glass transition of the PS matrix is observed (inset of Figure S3b in the Supporting Information). The intensity of the Bragg reflection decreases strongly (Figure S3c in the Supporting Information), which is consistent with the expected loss of contrast when both, the PDMS nanodomains and the PS matrix take up solvent. Initially, the scattering patterns do not change significantly, i.e., the film features randomly oriented cylinder nanodomains, but after ≈1200 s, the ring splits up into distinct reflections (**Figure 4**, red circles at 2570 s). These indicate the presence of lying cylinders on two hexagonal lattices, which have their *a*-directions oriented either along the film normal or lying in the film plane, as observed previously.[26] It is, at present, unclear whether the domains featuring these orientations are separated in the lateral direction or along the film normal, which is related to the question how they have appeared and grown, and why these two distinct orientations are favored over other ones.

The resulting reduced volumes (Figure 3b) show that toluene swells PS and PDMS nearly equally with a slight preference for PS: At the end of this swelling step, the reduced volumes of toluene are ≈1.31 in PS and 1.11 in PDMS. $\nu_{hep(PDMS)}$ and $\nu_{hep(PS)}$ are very close to zero, as expected, since no *n*-heptane is used so far. In the corresponding diagram of states (Figure 3c), this leads to a trajectory which runs predominantly down along the ϕ_P axis (down to 0.43) with the effective volume fraction of the PDMS nanodomains, f_{eff}, decreasing to 0.34.

During the exchange of toluene by *n*-heptane (3000–3900 s after the start), the swelling ratio continues to increase to a value of 2.3 (Figure 3a), the repeat distance and the grain size remain constant (Figure S3b,c in the Supporting Information, and the reflections in the 2D GISAXS maps, i.e., the cylinder orientation, are unchanged (Figure 4). Thus, no morphological changes are observed. The reduced volumes show that, while toluene continues to enter both domains, reaching values of 1.37 in PS and 1.17 in PDMS, *n*-heptane does not seem to enter the film, as evident from the close to zero values of ν_{hep}(PS) and ν_{hep}(PDMS). The reasons may be the following: i) The rather low overall flow rate of 50 sccm means that a complete gas exchange in the sample chamber takes as long as ≈180 s, which is a significant fraction of the 900 s allocated for the vapor exchange and leaves too little time for structural rearrangements. ii) Since the PDMS matrix is already swollen by toluene, the driving force for *n*-heptane to enter it as well is reduced compared to entering the dry PDMS nanodomains, resulting in a slow replacement of toluene by *n*-heptane in the film. The small changes of the volume fraction of toluene in the two types of nanodomains result in a slight sideward motion of the trajectory toward higher f_{eff} values (to ≈0.35).

During drying (3900–5110 s), S_R drops rapidly to ≈1.1 within ≈250 s, then decreases more slowly and reaches a value of 1.0 at the end of the run. The cylinder orientation rapidly gets lost, as evident from the more isotropic intensity distribution in the 2D GISAXS maps. The predominantly parallel orientation of the cylinders with two distinct orientations of the *a*-direction of the hexagonal lattice has changed to parallel (lying) cylinders with

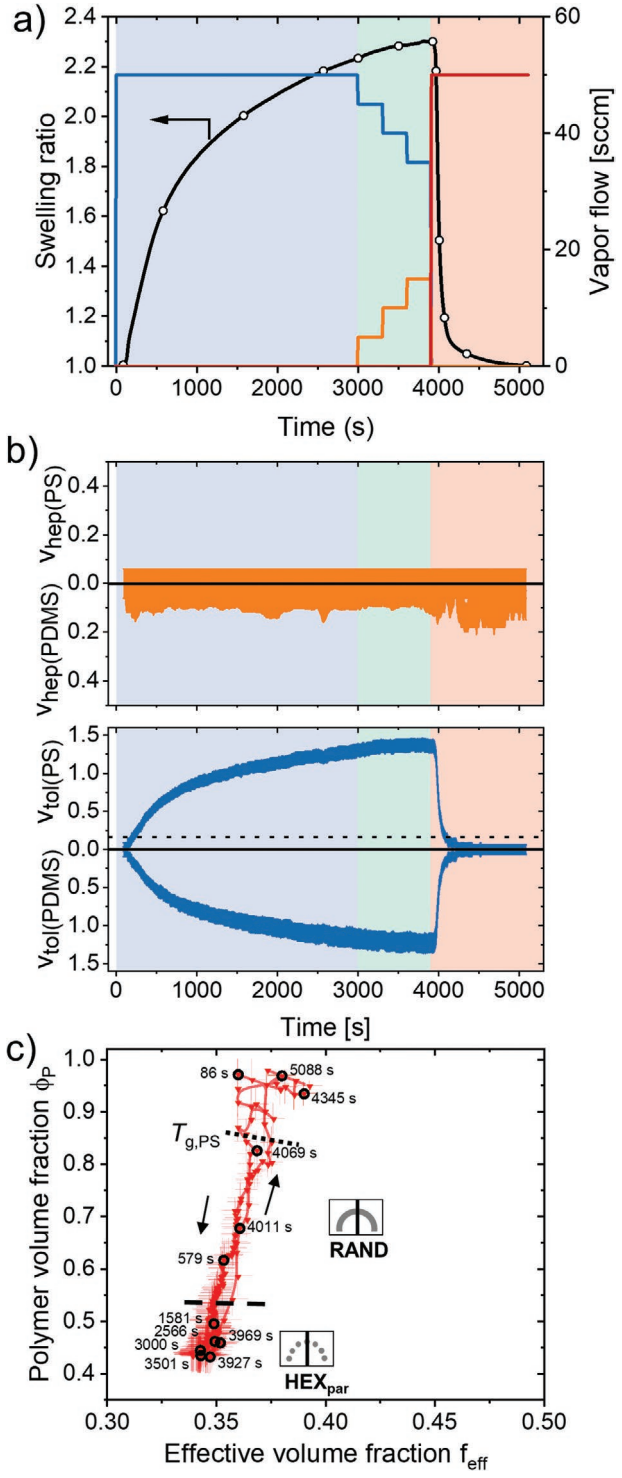

Figure 3. Protocol (ii). a) Variation of the vapor flows (brown: *n*-heptane, blue: toluene, red: pure N_2 gas, all right axis) and the resulting overall swelling ratio S_R (left axis) with time. Open circles indicate the times of selected 2D GISAXS maps shown in Figure 4 and Figure S3 in the Supporting Information. b) Reduced volumes of *n*-heptane and toluene in the PDMS nanodomains and the PS matrix. The value of $v_{tol(PS)}$ at which PS crosses the glass transition is indicated by a dotted line. c) The trajectory of the system during SVA. The times after the beginning of the experiment are given in the graph. The times at which the glass transition of PS is crossed upon swelling and drying (b) are indicated by a dotted line. The morphology changes from randomly oriented cylinders (RAND) until ≈1200 s to lying cylinders (HEX_{par}) up to ≈4000 s and back to randomly oriented afterward, as indicated by the schematic 2D GISAXS maps. The transition is indicated by the dashed line. Error bars are shown for every second data point. Open circles indicate the times of the 2D GISAXS maps and intensity profiles shown in Figure 4 and Figure S3 (Supporting Information).

a broad orientational distribution of the *a*-direction. The repeat distance increases rapidly (within 150 s) to ≈39.7 nm, which is significantly higher than the initial value. The reduced volumes of toluene go to zero within ≈250 s. Interestingly, as soon as toluene leaves the film, *n*-heptane enters the PDMS cylinders to a small extent, as seen from the finite values of v_{hep}(PDMS) (below ≈0.15). These changes in solvent distribution lead to an upward movement of the trajectory, reaching $\phi_P = 0.97$ and $f_{eff} = 0.38$ at the end of the run.

Thus, swelling the film in toluene vapor before exposing it to a 3:7 mixture of *n*-heptane/toluene vapors for 900 s results in a reorientation of the cylinders from random to parallel. The *a*-axis of the hexagonal lattice of these parallel cylinders assumes two distinct orientations in pure toluene vapor and in the *n*-heptane/toluene vapor mixture. The lamellar morphology is not reached, possibly due to the relatively short time, during which *n*-heptane is allowed to enter the film. Drying results in a loss of orientation of the *a*-axis.

Protocol (iii): To give the sample more time to absorb *n*-heptane vapor by being exposed to a vapor having an *n*-heptane/toluene ratio of 3:7 for longer time, protocol (ii) was repeated, but after swelling in pure toluene for 3000 s, toluene was fully exchanged by *n*-heptane in 10 steps of 300 s. Subsequently, the sample was kept in the vapor of pure *n*-heptane for 960 s, and a vapor having an *n*-heptane/toluene ratio of 3:7 was installed once more for 1170 s, before the film was dried rapidly (**Figure 5**a). We expected that the lamellar morphology would appear during the later stages of the protocol, when the PS matrix has been plasticized by swelling in toluene and when *n*-heptane has had sufficient time to enter the PDMS nanodomains.

The structural changes during the initial swelling step in toluene resemble strongly the ones in protocol (ii): S_R increases to a value of 2.1. During the first 1000 s of swelling, the lateral repeat distance increases from 28.9 to ≈34.5 nm and further to ≈36.0 nm during the remaining time (Figure S4b and Table S3 in the Supporting Information). The lateral grain size increases rapidly from its initial value of ≈108 to ≈150 nm after 550 s (Figure S4b in the Supporting Information). The initial 2D patterns corresponding to randomly oriented cylinders change after ≈1800 s to those indicating the presence of lying cylinders on two hexagonal lattices (**Figure 6**), as in protocol (ii). The intensity of the Bragg reflection decreases (Figure S4c in the Supporting Information), as in protocol (ii). This loss of contrast is reflected in the reduced volumes (Figure 5b), which show that toluene swells PS and PDMS nearly equally with only a slight preference for PS. Note that, at ≈300 s, *n*-heptane is present in the film for a short period of time, which we attribute to leftover *n*-heptane in the tubes from a previous experiment and which leads to a temporary increase of the intensity of the

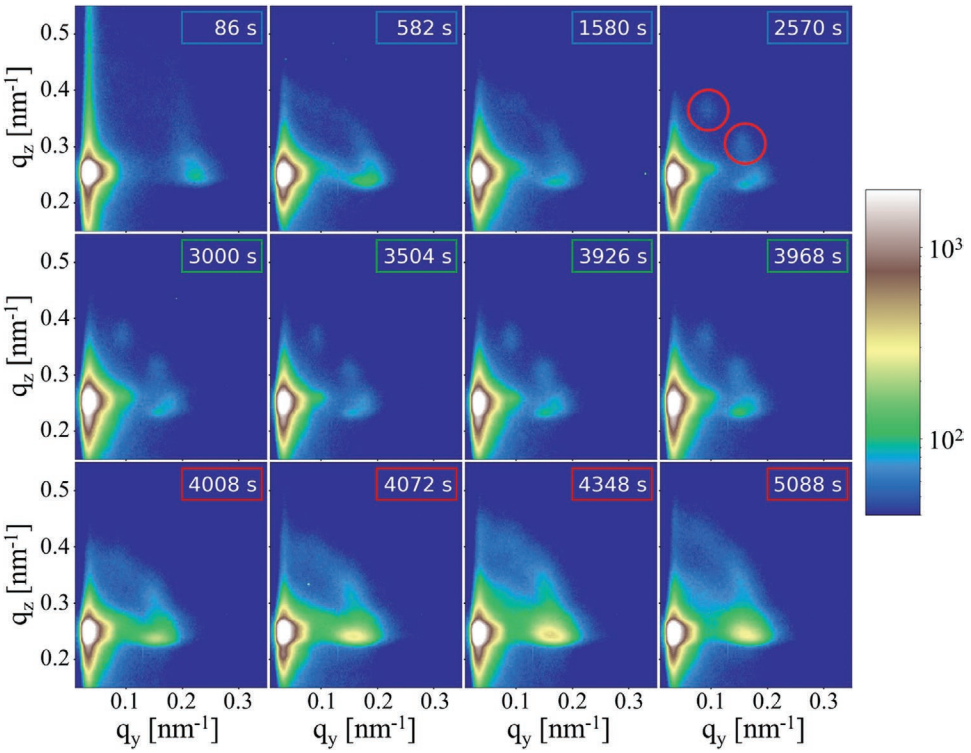

Figure 4. Protocol (ii). Selected measured 2D GISAXS maps at the times given. Colored frames around the times indicate the three stages of the protocol: blue: swelling in toluene, green: exchange of toluene by *n*-heptane until a ratio *n*-heptane/toluene of 3:7 is reached, red: drying. The scale bar gives the logarithmic intensity color map.

Bragg reflections. At the end of the swelling step, the reduced volumes of toluene are ≈1.21 in PS and 1.02 in PDMS, and no *n*-heptane is present in the film, as expected. In the diagram of states (Figure 5c), this corresponds to a downward trajectory along the ϕ_P axis (down to 0.47) with the effective volume fraction of the PDMS nanodomains, f_{eff}, decreasing to 0.34. Due to the short surge of *n*-heptane, f_{eff} briefly increases at ≈300 s.

During exchange of toluene by *n*-heptane and the subsequent time in pure *n*-heptane, S_R first increases to 2.13, which may be a consequence of the still high toluene content of the vapor, then decreases to 1.54, as the *n*-heptane content increases, and finally increases to 1.78. While this behavior is complex, the overall decrease compared to the value in pure toluene is consistent with the strong selectivity of *n*-heptane for the minority phase PDMS. The lateral repeat distance increases to ≈50.0 nm during several stages having different rates. The grain size decreases smoothly to ≈120 nm. Strong restructuring seems to proceed in the film, which is corroborated by the 2D maps (Figure 6, 3753–6249 s). The distinct reflections from the parallel cylinders on two hexagonal lattices merge (see the map at 5421 s). The scattering intensity increases strongly (the peak height increases by a factor of ≈60 between 3000 and 6900 s), which is attributed to the highly selective uptake of *n*-heptane by the PDMS cylinders. Moreover, the real part of the refractive index of *n*-heptane is smaller than the ones of all other components, which further enhances the contrast.[26]

At the same time, weak and broad second-order reflections appear (Figure S4a in the Supporting Information), which may indicate a transitional structure, expected to be finally transforming into the lamellar morphology. No reflection at the position $2q_{y,L}$*, which would be expected for the lamellar structure, is observed. However, from ≈4300 to ≈5400 s, the second-order reflection could be fitted by a Lorentzian peak located at $2^{1/2}$ $q_{y,L}$*. Its amplitude increases with time (Figure S5 in the Supporting Information). After 5400 s, an additional Lorentzian at $3^{1/2}$ $q_{y,L}$* had to be added as well. The amplitudes of both higher order reflections increase at the same pace during these two swelling steps. The presence of higher order reflections may indicate which morphology is encountered during the transition from the hexagonal to the lamellar state. In the phase diagrams of diblock copolymers, the (bicontinuous) gyroid phase appears between the hexagonal and the lamellar morphology.[45] However, the first higher-order reflection of the gyroid structure is expected to appear at $(4/3)^{1/2}$ $q_{y,L}$*,[46] which is lower than observed in the present data. Another possibility is the hexagonally perforated lamellar (HPL) structure, which consists of hexagonally perforated lamellar stacks. It was previously found that the HPL morphology may be an intermediate state in the transition from the cylindrical to the gyroid morphology.[47] For the HPL structure, reflections at positions of 1.88 $q_{y,L}$* are expected.[48] Given that, before the transition, the cylinders were aligned, one might expect that the emerging, transitional structures should feature an epitaxial relationship with the initial cylinders. However, the 2D GISAXS maps do not show distinct reflections, but rings. This may be due to fluctuations in the film, in which both domains now contain solvent (see below), and thus azimuthal smearing of the (numerous) first-order reflections in the gyroid or HPL structure.[46,48] Still,

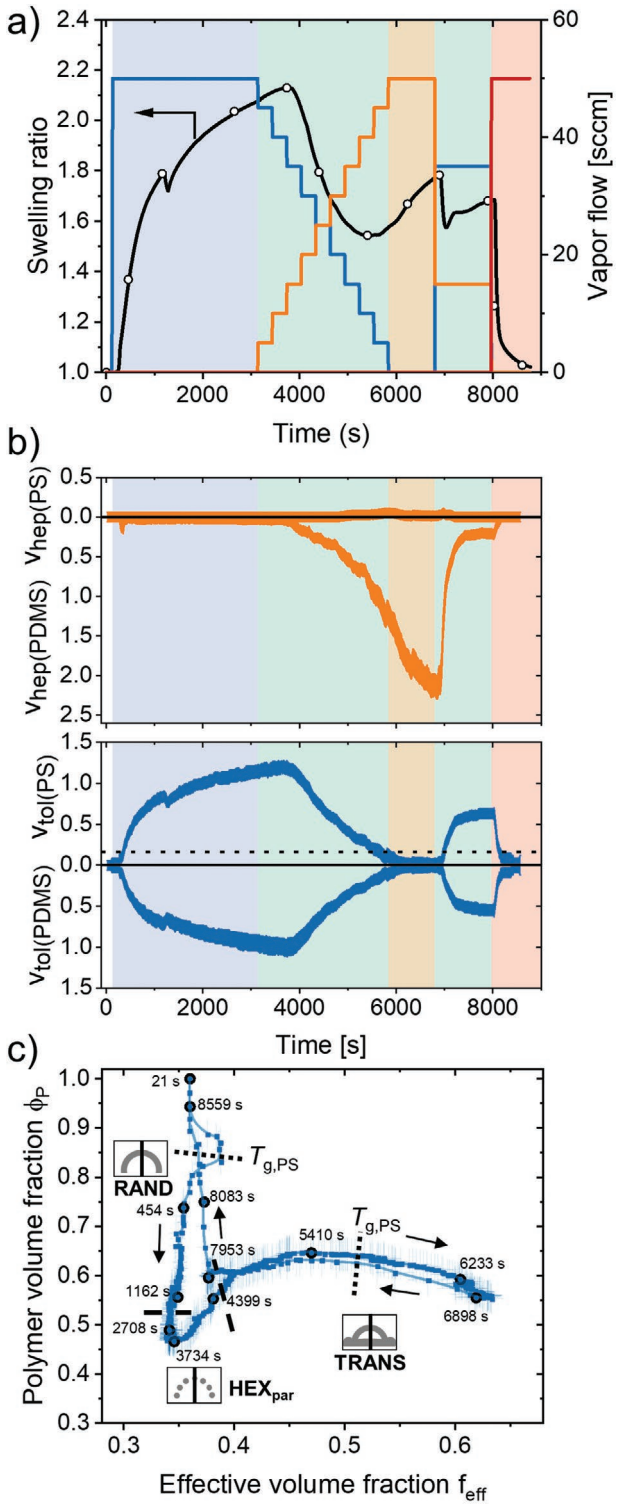

Figure 5. Protocol (iii). a) Variation of the vapor flows (brown: *n*-heptane, blue: toluene, red: pure N_2 gas, all right axis) and the resulting overall swelling ratio S_R (left axis) with time. The dip of S_R at 1280 s may be due to an instability of the fitting algorithm of the spectral reflectometer. Open circles indicate the times of selected 2D GISAXS maps and intensity profiles in Figure 6 and Figure S4 in the Supporting Information. b) Reduced volumes of *n*-heptane and toluene in the PDMS nanodomains and the PS matrix. The value of $\nu_{tol(PS)}$ at which PS crosses the glass transition is indicated with a dotted line. c) The trajectory of the system during SVA. The times at which the glass transition of PS is crossed upon swelling and drying (b) are indicated by a dotted line. The morphology changes from randomly oriented cylinders (RAND) up to ≈1800 s to lying cylinders (HEX_{par}) up to ≈4300 s, then to a transitional state (TRANS) up to ≈7400 s and back to randomly oriented afterward, as indicated by the schematic 2D GISAXS maps. The transitions are indicated by dashed lines. Error bars are shown for every second data point. Open circles indicate the times of the 2D GISAXS maps shown in Figure 6 and Figure S4 in the Supporting Information.

we conclude that the transition from cylinders to lamellae proceeds via a 3D structure, e.g., the HPL and gyroid morphology.

During the exchange and the exposure to pure *n*-heptane, $\nu_{tol(PS)}$ and $\nu_{tol(PDMS)}$ decrease and reach zero, and $\nu_{hep(PS)}$ remains close to zero, as expected. In contrast, $\nu_{hep(PDMS)}$ increases to values as high as 2.2; thus, the PDMS cylinders are strongly swollen by *n*-heptane. Interestingly, in contrast to protocol (ii), *n*-heptane can enter the film, when introduced into the sample cell over longer time and in larger amounts. Due to the uptake of *n*-heptane into the PDMS nanodomains, the trajectory reaches out to f_{eff} values as high as 0.63 (and ϕ_P = 0.55), i.e., significantly further toward the symmetric composition than in protocols (i) and (ii).

Due to the removal of toluene, the PS domain is expected to become glassy at ≈5700 s (indicated in Figure 5c with a dotted line). Thus, after the beginning of the morphological transition at ≈4300 s, the PS matrix was in a mobile state for ≈1400 s, allowing for structural rearrangements to take place. Afterward, the timescales of the structural changes were significantly increased. Since we do not observe a full transition from cylinder to lamellae, we can conclude that this time is not sufficient, and the film is trapped in a transitional state. Possibly, the lamellar state would have been achieved if a certain toluene flow had been maintained to keep the PS matrix plasticized. Bai et al. observed the appearance of the lamellar state during prolonged swelling of a PS-*b*-PDMS film in 5:1 *n*-heptane/toluene liquid mixtures (30 min of swelling for a sample with a molar mass of 12.2 kg mol^{-1}, which is significantly lower than the one used by us).[44]

Installing subsequently a vapor having a *n*-heptane/toluene ratio of 3:7 for 1170 s results in an S_R value of 1.68 at the end of the swelling step. The lateral repeat distance decreases abruptly to a value of 41.6 nm, while the grain size increases and settles at ≈140 nm. The reduced volume of *n*-heptane in PS stays at zero, whereas it decreases to 0.21 in PDMS. The reduced volumes of toluene in PS and PDMS go to 0.64 and 0.55, respectively. Due to the uptake of toluene, the PS matrix crosses the glass transition at ≈7000 s and becomes mobile. The morphology changes back to lying cylinders at ≈7400 s with no obvious preferential orientation (see, e.g., Figure 6, 7963 s), which is accompanied by an abrupt decrease of the peak intensity as well as an abrupt weakening of the higher-order reflections, especially the one at $3^{1/2}$ q^* (Figures S4a and S5 in the Supporting Information). The trajectory moves back to smaller f_{eff} values (0.38), while ϕ_P increases slightly to 0.60.

During drying, S_R decreases to 1 within ≈900 s, and the morphology is unchanged (randomly oriented cylinders), except an extension of the ring of scattering along the q_z axis, which is

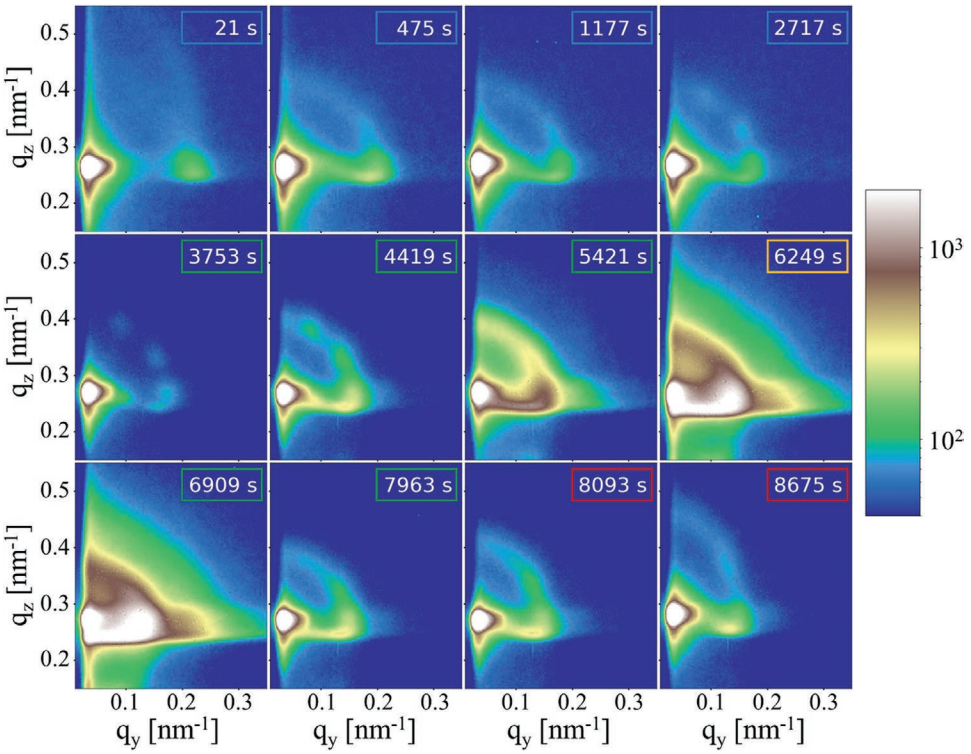

Figure 6. Protocol (iii). Selected measured 2D GISAXS maps at the times given. Colored frames around the times indicate the 5 stages of the protocol: blue: swelling in toluene, green: toluene/*n*-heptane exchange, brown: swelling in *n*-heptane, green: swelling in *n*-heptane/toluene at a ratio 3:7, red: drying. The scale bar gives the logarithmic intensity color map.

due to a decrease of the lattice spacing along the film normal upon the fast decrease of film thickness. The reduced volumes of *n*-heptane and toluene in the PS and PDMS nanodomains go to zero. The reflection at $2^{1/2}$ q^* is still present, albeit weak. The trajectory nearly reaches the starting point.

Comparing the trajectories and the morphologies obtained on the way for the different protocols (i.e., the three protocols discussed above as well as the one discussed in the Supporting Information of ref. [26]) allows us to construct a comprehensive diagram of states and to discuss the conditions needed to obtain a certain morphology as well as the role of the pathway. Details about the film presented in ref. [26] are given in the Supporting Information (Figures S6–S9, Supporting Information). Briefly, it featured initially randomly oriented lamellae. It was swollen in *n*-heptane for 3000 s; afterward, *n*-heptane was exchanged by toluene in 10 steps of 300 s each (all at room temperature, as in the present work). Upon swelling in *n*-heptane, the morphology stays unaltered. Upon exchange of *n*-heptane by toluene, the lamellar morphology is encountered, which is possible because PS crosses the glass transition and becomes viscoelastic. Both, parallel and perpendicular lamellae are present, which may be due to preferential surface wetting of PDMS at the film–air interface (parallel lamellae), whereas the substrate is neutral (vertical lamellae).[26] Finally, cylinders reappear. First, lying and standing cylinders coexist, and later, the lying orientation dominates with a very weak order.

In **Figure 7**, the locations of the morphological changes and glass transitions are compiled along with a schematic representation of the region accessed in the four trajectories. The latter is delimited by the trajectories of swelling in pure toluene (protocols (ii) and (iii)), in pure *n*-heptane (the film from ref. [26]) and the solvent exchange. The red line indicates the glass transition

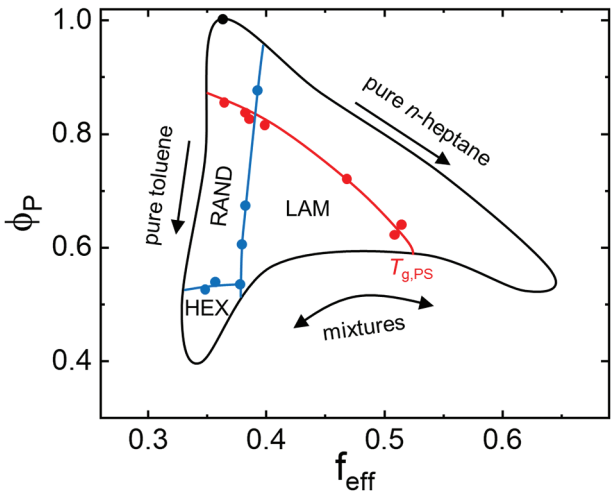

Figure 7. Diagram of states of PS-*b*-PDMS thin films swollen in toluene/*n*-heptane solvent vapor mixtures as a function of the effective volume fraction of the PDMS nanodomains, f_{eff}, and the volume fraction of polymer in the swollen film, ϕ_p. Red circles indicate the glass transitions of the PS matrix determined from the four SVA runs. Blue circles indicate observed morphology transitions. The various regions of morphologies are separated by solid blue lines and include randomly oriented cylinders (RAND), hexagonally ordered cylinders (HEX) and lamellae (LAM). The solid black line comprises the region of accessible states of the system, see text.

of the PS matrix, i.e., it is glassy above and mobile below. This shows that it is necessary to add toluene to make the PS matrix mobile. Three morphology regions are discerned, in agreement with other work on similar systems:[14,43,44] randomly oriented cylinders (i.e., the initial state), hexagonally ordered and oriented cylinders, and oriented lamellae. The transition from randomly to ordered and oriented cylinders takes place when ϕ_P falls below ≈0.5. The reason is at present unclear, possibly surface tension effects are at the origin of this transition. Others have reported similar trends.[13,43] The transition from cylinders to lamellae starts at $f_{eff} \cong 0.40$, but is sometimes hampered by the slow kinetics: When swelling in pure *n*-heptane (film from ref. [26]), the transition could not be completed, because the matrix was glassy the entire time.

The lamellar state with mobile PS nanodomains is only entered during the solvent exchange in protocol (iii) and for the film from ref. [26]. In protocol (iii), the film features hexagonally ordered cylinders in a mobile matrix before crossing the phase transition line and is in the mobile lamellar state for ≈1400 s, before it crosses the glass transition line upon further increase of the *n*-heptane content. After the solvent exchange, however, the lamellar morphology is not fully formed, but only a transitional state is encountered. A similar situation is encountered for the film in ref. [26] after swelling in *n*-heptane. However, the transitional state with the matrix being glassy can be transformed into lamellae upon increasing the toluene content and making the matrix mobile. The film is in the mobile lamellar region for ≈1300 s, before it reaches the phase transition line toward cylindrical morphologies.

Thus, it seems that is kinetically easier for the film to reach the lamellar state from the randomly oriented transitional state (as is the case in the trajectory of the film from ref. [26]) than from highly oriented, parallel cylinders (protocol (iii)). Even though they grow from the randomly oriented transitional state, the lamellae in the sample from ref. [26] feature two distinct orientations, namely the parallel and the perpendicular one. We have previously attributed these two lamellar orientations to preferential surface wetting of PDMS at the film–air interface (parallel lamellae), whereas the substrate is neutral (perpendicular lamellae).[26]

The region of hexagonally oriented cylinders is entered in protocols (ii) and (iii), and in the film from ref. [26]. In the former case, the films feature purely lying cylinders. In the latter case, a morphology featuring both standing and lying cylinders forms. We conclude that the orientation of the cylinders in this region depends strongly on the trajectory: Coming from the randomly oriented state (swelling in pure toluene or mixtures with a small fraction of *n*-heptane) promotes lying cylinders. Coming from the lamellar state (first swelling in *n*-heptane and then exchanging by toluene) promotes the coexistence of standing and lying cylinders. On the time scales of the experiment, these morphologies are stable, i.e., they are rather long-lived (minutes to hours).

To summarize, we used mixtures of *n*-heptane and toluene vapor to carry out solvent vapor annealing of PS-*b*-PDMS thin films featuring PDMS cylinders in a PS matrix. The close to nonselective toluene and the PDMS selective *n*-heptane were used with the aim of elucidating the role of the processing protocol on the swelling ratio, the morphology and its orientation, the lateral repeat distance, and the grain size. Making use of the procedure developed by us earlier,[26] we estimate the distribution of the two solvents among the PDMS and the PS nanodomains from the swelling ratio and the intensity of one of the Bragg reflections. From these, the effective volume fraction of the PDMS-rich phase and the overall polymer volume fraction are calculated, and the morphologies deduced from the Bragg reflections in the 2D GISAXS maps are related to these parameters. Moreover, the glass transition of the PS matrix is pinpointed from its toluene content. From the results, a comprehensive diagram of states is constructed for the PS-*b*-PDMS/toluene/*n*-heptane system, compiling the accessible morphologies and the regions where the matrix is glassy. This diagram may serve as a guideline to identify suitable SVA conditions in other systems.

Furthermore, we find that the sequence of the solvent introduction and exchange plays an important role. For instance, swelling the cylinders first does not lead to the expected transition to the lamellar morphology when the matrix is in the glassy state, only when it becomes mobile. This implies that the time needed for structural changes can be shortened significantly when keeping the matrix in a sufficiently swollen and thus mobile state. We have shown here that following a precise processing protocol is crucial, in order to achieve good ordering in such a complex system comprising two blocks and two solvents.

Experimental Section

Materials: The same cylinder-forming diblock copolymer, PS-*b*-PDMS as previously was used (Polymer Source Inc.).[26] Its block molar masses are 26.0 (PS) and 13.5 kg mol^{-1} (PDMS), i.e., the volume fraction of PDMS is $f = 0.36$. The χN value at room temperature is estimated to 86.[7] The glass transition temperatures of PS and PDMS are ≈100 °C and −124 °C, respectively. Thin films were prepared by spin-coating from an 8 wt% solution in propylene glycol monomethyl ether acetate on Si substrates, which had been pre-cleaned in an acid bath.[49,50] The thicknesses of the 3 films investigated were between 179 and 200 nm. For SVA, toluene and *n*-heptane were used. At 25 °C, their vapor pressures are 37.9 and 60.1 mbar.

SVA Setup: The experimental setup was similar to the one used in our previous work.[26] Briefly, a nitrogen gas flow was split into 3 parallel gas flows, passing through mass flow controllers (Bronkhorst High-Tech B.V.). Two of these gas flows were saturated in bubblers with the vapors of toluene and *n*-heptane, respectively. The third flow, pure nitrogen gas, was used for film drying. The three gas flows were mixed and directed to the sample cell, which had a volume of ≈150 cm^3 and was equipped with Kapton windows for X-ray measurements. A fiber optics entry embedded into the lid having a glass window enabled tracking of the film thickness in dependence on time, $h(t)$, using a FilMetrics F30 spectroscopic reflectometer. The swelling ratio is $S_R(t) = h(t)/h_0$, where h_0 is the initial film thickness. In all three experiments, the total gas flow through the experimental chamber was kept constant at 50 sccm (i.e., lower than in our previous experiments[26]) to reduce the swelling rate of the films. All experiments were carried out at room temperature.

GISAXS Experiments: GISAXS experiments were carried out at beamline D1 at the Cornell High Energy Synchrotron Source (CHESS) at Cornell University, Ithaca, USA, using a wavelength $\lambda = 0.1155$ nm and a beam size of 0.5 × 0.2 mm^2. The detector was a Medoptics CCD camera (pixel size 47 µm) at a sample-to-detector distance of 1845 mm, resulting in a q-resolution of 1.383×10^{-3} nm^{-1} pixel^{-1}. To protect the detector, the intense reflected beam as well as the intense scattering in the incident plane were blocked by a rod-shaped beam stop. The critical angles of total

external reflection are $\alpha_{c,film} \approx 0.11°$ and $\alpha_{c,substrate} \approx 0.17°$ for the dry PS-*b*-PDMS film and the Si substrate, respectively. GISAXS measurements were performed every 15–20 s for 0.3–0.5 s at an incident beam angle $\alpha_i = 0.14°$, i.e., the scattering pattern originates from the full depth of the polymer film. After each measurement, the sample chamber was moved sideward to expose a fresh sample area and thus avoid beam damage. The distance of the actual illuminated spot to the vapor inlet varied, resulting in slightly different conditions for consecutive images in a time-series, which is especially visible when the spot location changes from one side of the sample to the other. The *q*-calibration was done using Ag-behenate.

Analysis of GISAXS Maps: GISAXS provides a 2D distribution of the scattered radiation as a function of the scattering vector $\mathbf{q} = (q_x, q_y, q_z)$. To a good approximation, q_y and q_z point along the horizontal and the vertical axis of the detector plane, respectively. The 2D maps feature Debye–Scherrer-like rings, which in some cases, split up into distinct Bragg reflections. To extract the type of morphology, the lateral repeat distance and the compositions of the solvent-swollen PDMS nanodomains and the PS matrix from the experimentally obtained 2D GISAXS maps, the same procedures as in ref. [26] were followed. 1D intensity profiles were constructed by integrating the intensity along q_y over a narrow q_z range (5 pixels on the detector) around the q_z value of the specularly reflected beam, which is $q_z \cong 0.265$ nm^{-1}. For a detailed description, see the Supporting Information. The following expression was fitted to the intensity profiles

$$I(q_y) = \frac{I_L}{1+\left[\left(q_y - q_{y,L}^*\right)/w_L\right]^2} + I_G \exp\left[-\ln(2)\left(\frac{q_y - q_{y,G}^*}{w_G}\right)^2\right] + \frac{I_P}{q_y^\alpha} + I_{bg} \quad (1)$$

It contains a Lorentzian having the peak height I_L, the peak position $q_{y,L}$*, and the peak width w_L. It describes the first-order Debye–Scherrer ring/Bragg reflection around the specularly reflected beam. In some cases, the scattering around the direct beam is present in the intensity profiles as well, where it gives rise to a broad peak. (For a schematic representation, see the Supporting Information.) In some cases, this contribution overlaps with the first-order Bragg reflection of interest and hampers its precise characterization. It is modeled by an additional Gaussian having the amplitude I_G, the center position $q_{y,G}$* and the width w_G. The decaying background due to the diffuse scattering around the specularly reflected beam is empirically described by a power law with the amplitude I_P and the exponent α (which is typically between 3 and 4) and a constant background I_{bg}. The repeat distance d was calculated from $q_{y,L}$* using Bragg's law

$$d = \frac{2\pi}{q_{y,L}^*} \quad (2)$$

and the lateral grain size G was estimated from the full width at half maximum, $\Delta q_y = 0.828\ w_L$ using the Scherrer equation[51,52]

$$G = \frac{2\pi K}{\Delta q_y} \quad (3)$$

where the constant K was set to the standard value of 0.9.[51]

The presence of higher-order reflections indicates improved long-range order of the nanodomains and/or a change in morphology. One higher-order peak was observed for protocol (iii) for times between 4000 and 5400 s and larger than 7050 s and two higher-order peaks for times between 5400 and 7050 s. These reflections were fitted using one or two additional Lorentzians, for details see the Supporting Information. For the other protocols, no higher-order peaks were observed.

From the swelling ratio of the film together with the area under the first-order Bragg reflection, the distribution of the two solvents among the two types of polymeric nanodomains was calculated following the same procedure as in ref. [26]: The reduced volumes of the solvents (k = *n*-heptane, hep, or toluene, tol) in the two types of nanodomains (p = PDMS or PS) are defined as

$$\nu_{k(p)} = \frac{V_k}{V_p} \quad (4)$$

where V_k denotes the volumes of *n*-heptane or toluene and V_p the volumes of PS or PDMS. According to this definition, the overall polymer volume fraction ϕ_P is related to the reduced volumes by

$$\phi_P = \left[f(1+\nu_{tol(PDMS)}+\nu_{hep(PDMS)}) + (1-f)(1+\nu_{tol(PS)}+\nu_{hep(PS)})\right]^{-1} \quad (5)$$

and the effective volume fraction of swollen PDMS, f_{eff}, by

$$f_{eff} = \frac{f(1+\nu_{tol(PDMS)}+\nu_{hep(PDMS)})}{(1-f)(1+\nu_{tol(PS)}+\nu_{hep(PS)}) + f(1+\nu_{tol(PDMS)}+\nu_{hep(PDMS)})} \quad (6)$$

To obtain the four reduced volumes from the experiments, four conditions were applied: ϕ_P was determined experimentally from the measured swelling ratio by $\phi_P = 1/S_R$. An experimental contrast factor was determined from the area under the first-order Bragg reflection and was related to the reduced volumes (Equations (3) and (7) in ref. [26]). Two boundary conditions were used to narrow down the possible states for a given pair of the swelling ratio and the contrast factor. These are based on previous swelling experiments, where only *n*-heptane or toluene was used for SVA.[26] *n*-heptane was assumed to be strongly selective for PDMS

$$0.0 \le \frac{\nu_{hep(PS)}}{\nu_{hep(PDMS)}} \le 0.1 \quad (7)$$

and toluene was assumed to be weakly selective for PS

$$0.7 \le \frac{\nu_{tol(PDMS)}}{\nu_{tol(PS)}} \le 1 \quad (8)$$

From the such obtained reduced volumes, f_{eff} is calculated by using Equation (6) which allowed us to draw the trajectory of the sample and the morphologies encountered during swelling, solvent exchange, and drying in dependence on f_{eff} and ϕ_P (called diagram of states). Uncertainties were determined as described in ref. [26].

The value of $\nu_{tol(PS)}$ at which PS crosses the glass transition during swelling and during drying was estimated to be 0.16 (details of the calculation can be found in the Supporting Information). The such obtained values of f_{eff} and ϕ_P at these points are marked in the diagram of states.

Supporting Information

Supporting Information is available from the Wiley Online Library or from the author.

Acknowledgements

The financial support from Deutsche Forschungsgemeinschaft (project PA 771/10-2, A.V.B. and C.M.P.) in the framework of the Memorandum of Understanding on Cooperation between DFG and RFBR is gratefully acknowledged. D.P. and T.B.T. thank DANSCATT (Danish Centre for the Use of Synchrotron X-ray and Neutron Facilities) for financial support. This work is based upon research conducted at the Cornell High Energy Synchrotron Source (CHESS), which is supported by the National Science Foundation award DMR-1332208. The authors thank CHESS for providing beamtime and excellent equipment.

Conflict of Interest

The authors declare no conflict of interest.

Keywords

block copolymers, thin films, grazing-incidence small-angle X-ray scattering, solvent vapor annealing, vapor mixtures

Received: March 24, 2020
Revised: May 15, 2020
Published online: June 17, 2020

[1] M. J. Fasolka, A. M. Mayes, *Annu. Rev. Mater. Res.* **2001**, *31*, 323.
[2] R. A. Segalman, *Mater. Sci. Eng., R* **2005**, *48*, 191.
[3] I. W. Hamley, *Prog. Polym. Sci.* **2009**, *34*, 1161.
[4] W. Li, M. Liu, F. Qiu, A. C. Shi, *J. Phys. Chem. B* **2013**, *117*, 5280.
[5] J. J. Walish, Y. Fan, A. Centrone, E. L. Thomas, *Macromol. Rapid Commun.* **2012**, *33*, 1504.
[6] D. Heinrich, M. Hufnagel, C. R. Singh, M. Fischer, S. Alam, H. Hoppe, T. Thurn-Albrecht, M. Thelakkat, in *Elementary Processes in Organic Photovoltaics*, Vol. 272 (Ed. K. Leo), Springer, Cham, Germany **2017**, p. 157.
[7] J. G. Kennemur, L. Yao, F. S. Bates, M. A. Hillmyer, *Macromolecules* **2014**, *47*, 1411.
[8] M. Li, C. K. Ober, *Mater. Today* **2006**, *9*, 30.
[9] R. Ruiz, H. Kang, F. A. Detcheverry, E. Dobisz, D. S. Kercher, T. R. Albrecht, J. J. De Pablo, P. F. Nealey, *Science* **2008**, *321*, 936.
[10] K. Brassat, D. Kool, J. Bürger, J. K. N. Lindner, *Nanoscale* **2018**, *10*, 10005.
[11] M. Müller, *Prog. Polym. Sci.* **2020**, *101*, 101198.
[12] Y. S. Jung, C. A. Ross, *Adv. Mater.* **2009**, *21*, 2540.
[13] M. Y. Paik, J. K. Bosworth, D.-M. Smilges, E. L. Schwartz, X. Andre, C. K. Ober, *Macromolecules* **2010**, *43*, 4253.
[14] K. W. Gotrik, A. F. Hannon, J. G. Son, B. Keller, A. Alexander-Katz, C. A. Ross, *ACS Nano* **2012**, *6*, 8052.
[15] C. Sinturel, M. Vayer, M. Morris, M. A. Hillmyer, *Macromolecules* **2013**, *46*, 5399.
[16] P. W. Majewski, K. G. Yager, *J. Phys.: Condens. Matter* **2016**, *28*, 403002.
[17] C. Jin, B. C. Olsen, E. J. Luber, J. M. Buriak, *Chem. Mater.* **2017**, *29*, 176.
[18] D. Posselt, J. Zhang, D.-M. Smilgies, A. V. Berezkin, I. I. Potemkin, C. M. Papadakis, *Prog. Polym. Sci.* **2017**, *66*, 80.
[19] K. W. Gotrik, C. A. Ross, *Nano Lett.* **2013**, *13*, 5117.
[20] J. M. Kim, Y. J. Kim, W. I. Park, Y. H. Hur, J. W. Jeong, D. M. Sim, K. M. Baek, J. H. Lee, M. J. Kim, Y. S. Jung, *Adv. Funct. Mater.* **2015**, *25*, 306.
[21] S. S. Dinachali, W. Bai, K. H. Tu, H. K. Choi, J. Zhang, M. E. Kreider, L. C. Cheng, C. A. Ross, *ACS Macro Lett.* **2015**, *4*, 500.
[22] D. T. Hoang, J. Yang, K. Paeng, Y. Kwon, O. S. Kweon, L. J. Kaufman, *Rev. Sci. Instrum.* **2016**, *87*, 015106.
[23] K. Kim, S. Park, Y. Kim, J. Bang, C. Park, D. Y. Ryu, *Macromolecules* **2016**, *49*, 1722.
[24] B. C. Stahl, E. J. Kramer, C. J. Hawker, N. A. Lynd, *J. Polym. Sci., Part B: Polym. Phys.* **2017**, *55*, 1125.
[25] R. Lundy, S. P. Flynn, C. Cummins, S. M. Kelleher, M. N. Collins, E. Dalton, S. Daniels, M. A. Morris, R. Enright, *Phys. Chem. Chem. Phys.* **2017**, *19*, 2805.
[26] A. V. Berezkin, F. Jung, D. Posselt, D.-M. Smilgies, C. M. Papadakis, *Adv. Funct. Mater.* **2018**, *28*, 1706226.
[27] G. Nelson, C. S. Drapes, M. A. Grant, R. Gnabasik, J. Wong, A. Baruth, *Micromachines* **2018**, *9*, 271.
[28] C. M. Papadakis, Z. Di, D. Posselt, D.-M. Smilgies, *Langmuir* **2008**, *24*, 13815.
[29] X. Gu, I. Gunkel, A. Hexemer, T. P. Russell, *Colloid Polym. Sci.* **2014**, *292*, 1795.
[30] A. Sepe, J. Zhang, J. Perlich, D.-M. Smilgies, D. Posselt, C. M. Papadakis, *Eur. Polym. J.* **2016**, *81*, 607.
[31] I. Gunkel, X. Gu, Z. Sun, E. Schaible, A. Hexemer, T. P. Russell, *J. Polym. Sci., Part B: Polym. Phys.* **2016**, *54*, 331.
[32] I. Saito, D. Shimada, M. Aikawa, T. Miyazaki, K. Shimokita, H. Takagi, K. Yamamoto, *Polym. J.* **2016**, *48*, 399.
[33] A. A. Rudov, E. S. Patyukova, I. V. Neratova, P. G. Khalatur, D. Posselt, C. M. Papadakis, I. I. Potemkin, *Macromolecules* **2013**, *46*, 5786.
[34] A. F. Hannon, W. Bai, A. Alexander-Katz, C. A. Ross, *Soft Matter* **2015**, *11*, 3794.
[35] S. P. Paradiso, K. T. Delaney, C. J. García-Cervera, H. D. Ceniceros, G. H. Fredrickson, *Macromolecules* **2016**, *49*, 1743.
[36] A. V. Berezkin, C. M. Papadakis, I. I. Potemkin, *Macromolecules* **2016**, *49*, 415.
[37] J. Hao, Z. Wang, Z. Wang, Y. Yin, R. Jiang, B. Li, Q. Wang, *Macromolecules* **2017**, *50*, 4384.
[38] F. S. Bates, G. H. Fredrickson, *Annu. Rev. Phys. Chem.* **1990**, *41*, 525.
[39] T. P. Lodge, B. Pudil, K. J. Hanley, *Macromolecules* **2002**, *35*, 4707.
[40] M. A. Chavis, D.-M. Smilgies, U. B. Wiesner, C. K. Ober, *Adv. Funct. Mater.* **2015**, *25*, 3057.
[41] K. Lee, M. Kreider, W. Bai, L.-C. Cheng, S. S. Dinachali, K.-H. Tu, T. Huang, K. Ntetskikas, G. Liontos, A. Avgeropoulos, C. A. Ross, *Nanotechnology* **2016**, *27*, 465301.
[42] C. M. Hansen, *Hansen Solubility Parameters: A User's Handbook*, 2nd ed., CRC Press, Boca Raton, FL **2007**.
[43] W. Bai, K. G. Yager, C. A. Ross, *Macromolecules* **2015**, *48*, 8574.
[44] W. Bai, K. G. Yager, C. A. Ross, *Polymer* **2016**, *101*, 176.
[45] M. W. Matsen, F. S. Bates, *Macromolecules* **1996**, *29*, 1091.
[46] M. E. Vigild, K. Almdal, K. Mortensen, I. W. Hamley, J. P. A. Fairclough, A. J. Ryan, *Macromolecules* **1998**, *31*, 5702.
[47] C.-Y. Wang, T. P. Lodge, *Macromolecules* **2002**, *35*, 6997.
[48] A. K. Khandpur, S. Förster, F. S. Bates, I. W. Hamley, A. J. Ryan, W. Bras, K. Almdal, K. Mortensen, *Macromolecules* **1995**, *28*, 8796.
[49] P. Müller-Buschbaum, *Eur. Phys. J. E* **2003**, *12*, 443.
[50] A. V. Berezkin, F. Jung, D. Posselt, D.-M. Smilgies, C. M. Papadakis, *ACS Appl. Mater. Interfaces* **2017**, *9*, 31291.
[51] P. Scherrer, *Nachr. Ges. Wiss. Göttingen* **1918**, *26*, 98.
[52] D.-M. Smilgies, *J. Appl. Crystallogr.* **2009**, *42*, 1030

